

Prediction of absolute rate coefficients and product branching ratios for the $C(^3P) + \text{allene}$ reaction system

Harold W. Schranz^{a)}

Institute of Atomic and Molecular Sciences, Academia Sinica, Taipei, Taiwan and Computational Molecular Science Group, Department of Chemistry, University of Queensland, St. Lucia, Qld 4072, Australia

Sean C. Smith^{b)}

Computational Molecular Science Group, Department of Chemistry, University of Queensland, St. Lucia, Qld 4072, Australia

Alexander M. Mebel^{c)} and Sheng H. Lin^{d)}

Institute of Atomic and Molecular Sciences, Academia Sinica, Taipei, Taiwan

(Received 31 January 2002; accepted 22 July 2002)

Complex chemical reactions in the gas phase can be decomposed into a network of elementary (e.g., unimolecular and bimolecular) steps which may involve multiple reactant channels, multiple intermediates, and multiple products. The modeling of such reactions involves describing the molecular species and their transformation by reaction at a detailed level. Here we focus on a detailed modeling of the $C(^3P) + \text{allene}$ (C_3H_4) reaction, for which molecular beam experiments and theoretical calculations have previously been performed. In our previous calculations, product branching ratios for a nonrotating isomerizing unimolecular system were predicted. We extend the previous calculations to predict absolute unimolecular rate coefficients and branching ratios using microcanonical variational transition state theory (μ -VTST) with full energy and angular momentum resolution. Our calculation of the initial capture rate is facilitated by systematic *ab initio* potential energy surface calculations that describe the interaction potential between carbon and allene as a function of the angle of attack. Furthermore, the chemical kinetic scheme is enhanced to explicitly treat the entrance channels in terms of a predicted overall input flux and also to allow for the possibility of redissociation via the entrance channels. Thus, the computation of total bimolecular reaction rates and partial capture rates is now possible. © 2002 American Institute of Physics. [DOI: 10.1063/1.1506307]

I. INTRODUCTION

This paper presents results of our new study of the $C(^3P) + \text{allene}$ (C_3H_4) reaction, for which experiments and theoretical calculations have previously been performed.¹⁻³ In the previous modeling, product branching ratios for a nonrotating isomerizing unimolecular system were predicted.²

In the current study, we have substantially extended the previous calculations in order to predict absolute unimolecular rate coefficients and branching ratios using microcanonical variational transition state theory (μ VTST) (Refs. 4-6) with full energy and angular momentum (E, J) resolution.⁶ The chemical kinetic scheme for the overall reaction is enhanced to explicitly treat the entrance channels in terms of a predicted overall input flux and also to allow for the possibility of redissociation via the entrance channels. Our calculation of the initial capture rate is facilitated by systematic potential energy surface (PES) calculations that describe the interaction potential between carbon and allene as a function

of the angle of attack. This approach goes beyond the assumptions inherent in simpler anisotropic models [e.g., free rotor and CSHR (Ref. 7)] and calculates the anisotropy for the entrance channel based on an explicit *ab initio* model of the PES.

Our motivation for this project is to understand the detailed reaction dynamics of complex reactions in the gas phase at a energy and angular momentum (E, J) resolved level. We then are able to predict both detailed quantities such as E, J -resolved product branching ratios $b_p(E, J)$ as well as averaged quantities of interest such as thermal bimolecular rate coefficients $k(T)$. Our goal is to construct a systematic theoretical treatment for such complex reactions,^{8,9} a goal indeed shared by other research groups.¹⁰⁻¹⁵

Complex chemical reactions (at least in the gas phase) can be decomposed into a network of elementary (e.g., unimolecular and bimolecular) steps which may involve multiple reactant channels, multiple intermediates, and multiple products. To each elementary step μ VTST is then applied to variationally predict the sum of states $W(E, J)$ and the unimolecular rate coefficient $k(E, J)$ and thus properly account for angular momentum conservation (thereby going beyond the usual microcanonical RRKM treatment in terms of just E). Improvements over previous approaches include a more rigorous treatment of transitional modes via use of an *ab*

^{a)}Electronic mail: Harold.Schranz@adfa.edu.au; Current address: School of Chemistry, University College (UNSW), Australian Defense Force Academy, Canberra ACT 2600, Australia.

^{b)}Electronic mail: S.Smith@chemistry.uq.edu.au

^{c)}Electronic mail: mebel@po.iam.s.sinica.edu.tw

^{d)}Electronic mail: hshaw@po.iam.s.sinica.edu.tw

initio PES and being able to variationally minimize the reactive flux with respect to (in principle) better definitions of the (generalized) reaction coordinate.⁶

A significant impetus to our goals is the considerable data provided by recent sophisticated experiments on a wide variety of complex reaction systems, e.g., $C(^3P) + C_3H_4$ (allene and propyne), $C_2 + C_2H_4$, $O + SiH_4$, $O + CH_3F$, $O(^1D) + CH_4$.^{1-3,16-18} For the present study we begin with our title system: $C(^3P) + \text{allene } (C_3H_4)$.

The $C(^3P) + \text{allene } (C_3H_4)$ reaction is an example of a class of hydrocarbon radical reactions that are of major importance in combustion chemistry,^{19,20} atmospheric chemistry²¹ and astrochemistry.²² It involves likely reaction pathways for formation of *i/n*- C_4H_3 isomers (implicated in aromatic ring formation in combustion). Some of the relevant (crossed molecular beam) experiments and theoretical (*ab initio* and RRKM) calculations performed at the IAMS on the $C(^3P) + \text{allene } (C_3H_4)$ system are described in Refs. 1-3.

In the following sections we briefly describe the $C(^3P) + \text{allene } (C_3H_4)$ system, in terms of the PES pathways between reactants, intermediates and products. The *ab initio* PES calculations for the entrance channel are presented. An enhanced chemical kinetic scheme for the overall reaction is constructed and solved. The application of μ VTST to prediction of the elementary rate constants is described. The computation of the typical time evolution of the system and the calculation of branching ratios and total bimolecular reaction rates is presented and discussed. Concluding remarks are made in the final section.

II. THE TRIPLET C_4H_4 POTENTIAL ENERGY SURFACE

A. Major species and pathways

The geometries and energies of various isomers of triplet C_4H_4 , transition states and dissociation products have been calculated in a previous study.^{2,3} The geometries in that study were optimized using the hybrid density functional B3LYP method²³ with the 6-311G(*d,p*) basis set. Energies were estimated using the higher level G2M(RCC,MP2) method.²⁴

The major triplet C_4H_4 PES pathways are shown in Fig. 1. For brevity, we give here just a brief description of the PES pathways as a detailed representation and discussion is given in the previous work.^{2,3} The significant intermediate species for the primary reaction pathways producing the major product *p1* and minor product *p2* are *i1*, *i3*, *i2*, and *i7*. There are two possible entrance channels, both without an entrance barrier. The major channel involves attack of the incoming carbon atom on either of the allenic double bonds to form species *i1*, a cyclic isomer (a triplet cyclopropylidene derivative) which is stabilized by 63.4 kcal/mol (265.3 kJ/mol) with respect to the reactants. The minor entrance channel involves an attack of the incoming carbon on the central allenic carbon to form species *i3*, a branched isomer (a triplet diradical) which is stabilized by 46.1 kcal/mol (192.9 kJ/mol) with respect to the reactants. Previous calculations² indicate that the species *i3* quickly converts to species *i1* (due to a small barrier of 12.6 kJ/mol) and the major

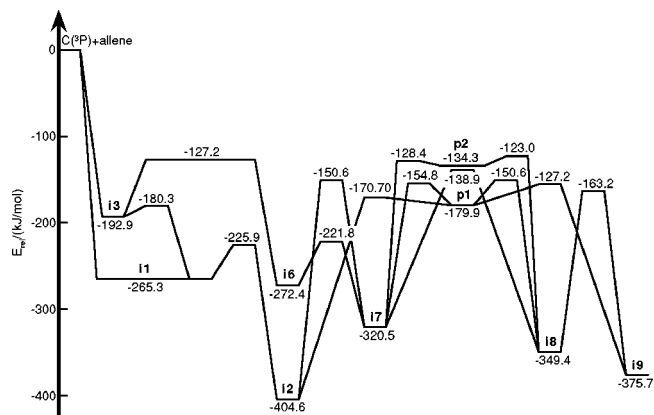


FIG. 1. Triplet C_4H_4 PES pathways. Energies include the zero-point energy and were estimated using the G2M(RCC,MP2) method (Ref. 24).

reaction channel is formation of product *p1* (*n*- C_4H_3) via the intermediate isomer *i2* (triplet butatriene) whereas product *p2* (*i*- C_4H_3) is formed in only minor amounts (about 1%). The *i2* isomer represents the global minimum of the triplet C_4H_4 PES and is bound by 96.7 kcal/mol (404.6 kJ/mol) with respect to the reactants. It can emit a H-atom to form *p1* or undergo a [1,2]-H migration to form *i7* (a C_4H_4 isomer) which can either fragment to form *p1* or *p2*. A much more minor pathway beginning with *i3* involves ring closure via a tight transition state with a significant forward barrier of 65.7 kJ/mol to form the C_4H_4 isomer *i6* which can ring open via a barrier of 50.6 kJ/mol to form *i7*. Much more detail on the intermediate species can be found in the previous work.^{2,3}

B. *Ab Initio* PES for anharmonic (transitional) modes

One aim of the current project is to incorporate reversible flux in the entrance channel into the chemical kinetic scheme of Ref. 2. Thus, in our code, UNIRATE,²⁵ the calculation has been updated to allow for the incorporation of the anisotropy for the entrance channel based on an explicit *ab initio* model of the PES. It is this more sophisticated treatment that is described below.

As with the previous calculations,^{2,3} our new *ab initio* calculations were performed via a density functional theory (DFT) approach, B3LYP/6-311G**, using the GAUSSIAN 98 program.²⁶ In the present calculations, PES scans over the internal coordinates (R, θ, ϕ), described in Fig. 2(a), were performed with all other coordinates frozen at the equilibrium allene configuration. This approximation was necessary to keep the amount of *ab initio* calculation tractable and should suffice for the purpose of estimating the anisotropy for the entrance channel. The grid of potential energies used covers center of mass separations of $R = 3.0$ – 6.0 Å at intervals of 0.2 Å and the angles θ and ϕ are sampled at 10° intervals over the range 0–90°.

Samples of the PES $V(R, \theta, \phi)$ are shown for a center-of-mass separation of $R = 3.0$ and 4.0 Å in Figs. 2(b) and 2(c). The repulsion felt by the incoming carbon atom by one of the allene hydrogens is clearly seen in Fig. 2(b) for angles of approach of ($\theta \approx 30^\circ, \phi \approx 0^\circ$) whereas attractive interaction

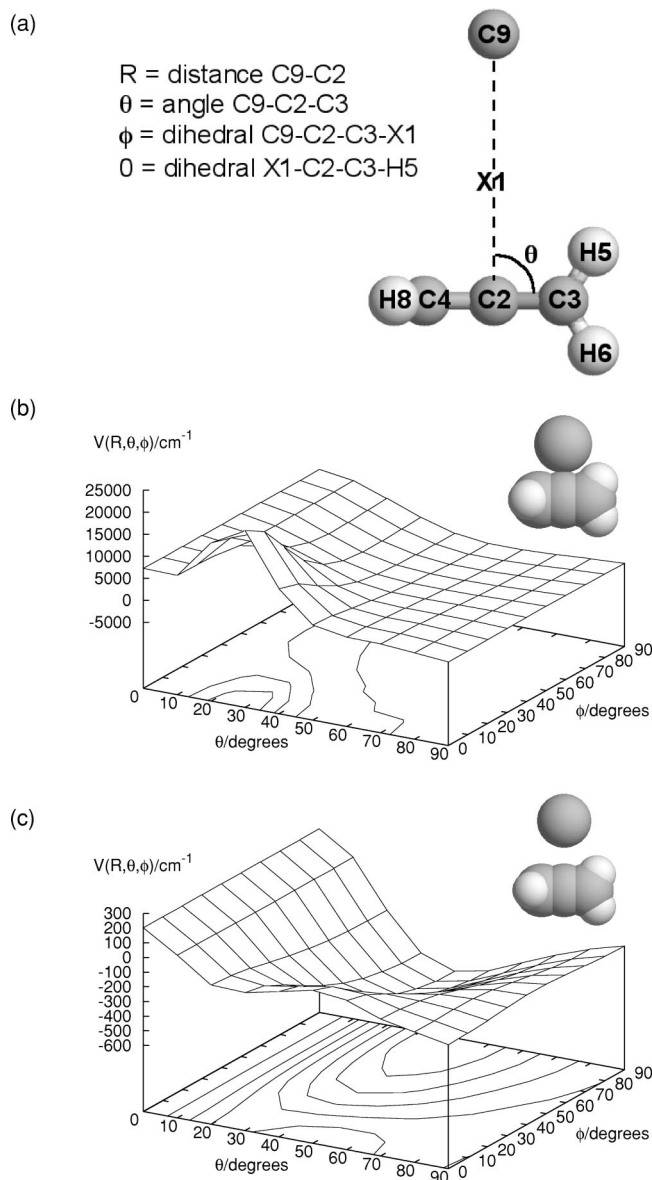


FIG. 2. (a) Definition of the coordinates (R, θ, ϕ) and the frozen dihedral (zero angle) used in the present calculations on C+C₃H₄ (allene). (b) The PES $V(R, \theta, \phi)/\text{cm}^{-1}$ at a separation of $R=3.0 \text{ \AA}$ for C+C₃H₄ (allene) based on *ab initio* calculations generated with GAUSSIAN 98. (c) As in (b) but at a separation of $R=4.0 \text{ \AA}$.

results from approach angles of ($\theta \approx 40-90^\circ$, $\phi \approx 90^\circ$), reflecting the potential for bonding to the allenic double bond or the central carbon atom. The PES $V(R_i, \theta, \phi)$ for each separation R_i , obtained above, were interpolated at each required separation R to yield a PES $V(R, \theta, \phi)$. For current purposes, it was found sufficient and robust to use linear interpolation.

These B3LYP/6-311G** energies were corrected by a simple scale factor, based on the difference between the B3LYP/6-311G** DFT and higher level G2M predictions for the well depth of the $i1$ species with respect to the reactants (C+allene), 70.96 and 65.75 kcal/mol, respectively. The resulting scale factor of 0.9266 was applied to the B3LYP/6-311G** DFT energies to yield the final PES used in our calculations.

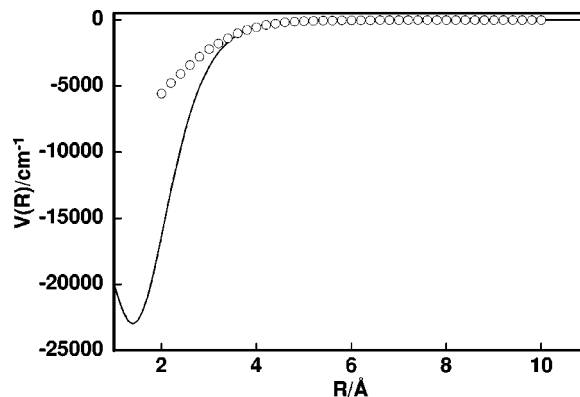


FIG. 3. MEP *ab initio* points and stiff Morse fit.

When calculating the microcanonical rate coefficient $k(E, J)$ (as described in Sec. IV) for the loose C+allene entrance/exit channels at low values of the energy E and angular momentum J , the variationally determined transition state location lies at large separations R which may exceed the range of our *ab initio* based PES. To remedy this, extension of the PES for center-of-mass separations R beyond 6.0 \AA was achieved by estimating the minimum energy path (MEP) for the C+allene entrance channel and using this information to apply a damping function to the existing PES to yield an asymptotically flat PES at long separations R .

Firstly, the MEP was estimated by fitting B3LYP/6-311G** DFT calculations at the longer center-of-mass separations of $R=4.0-10.0 \text{ \AA}$ as well as the minimum energy for entrance channel species $i1$ at $R=1.4 \text{ \AA}$. Fits were performed on the scaled *ab initio* energies (scaled by 0.9266 for B3LYP relative to G2M at the minimum) for consistency with the scaled PES potential. The fitted MEP was represented by a Stiff Morse functional form over the range $R_e < R < R_{\text{LIM}}$ with

$$V_{\text{MEP}}(R) = D_e \{1 - \exp[-\beta(R)]\}^2 - D_e, \quad (1)$$

$$\beta(R) = \sum_{i=1}^M a_i (R - R_e)^i. \quad (2)$$

The chosen parameters and fitted coefficients for the MEP are $D_e = 65.75 \text{ kcal/mol} = 22996 \text{ cm}^{-1}$, $R_e = 1.4 \text{ \AA}$, $R_{\text{LIM}} = 19.4 \text{ \AA}$, and the $M=5$ least squares fitted coefficients $a_1 = 1.004255$, $a_2 = 0.526404$, $a_3 = -0.121679$, $a_4 = 0.009174$, $a_5 = -0.000214$. The fitted MEP is shown in Fig. 3.

Using a damping function based on the decay function $\beta(R)$ from the fitted MEP Stiff Morse function in Eq. (1) the asymptotically damped PES can be formulated as

$$V(R, \theta, \phi) = \{V(R_{\text{CMX}}, \theta, \phi) - V_{\text{MEP}}(R_{\text{CMX}})\} \times \exp[-\beta(R) + \beta(R_{\text{CMX}})] + V_{\text{MEP}}(R), \quad (3)$$

where $R_{\text{CMX}} = 6 \text{ \AA}$ is the maximum center-of-mass separation R at which the *ab initio* PES is available. For consistency, the exponential damping term is set to zero for $R > R_{\text{LIM}}$, beyond which point the PES is essentially flat.

This PES model of the entrance channel is used also for the exit channels leading to dissociation of the $i1$ and $i3$

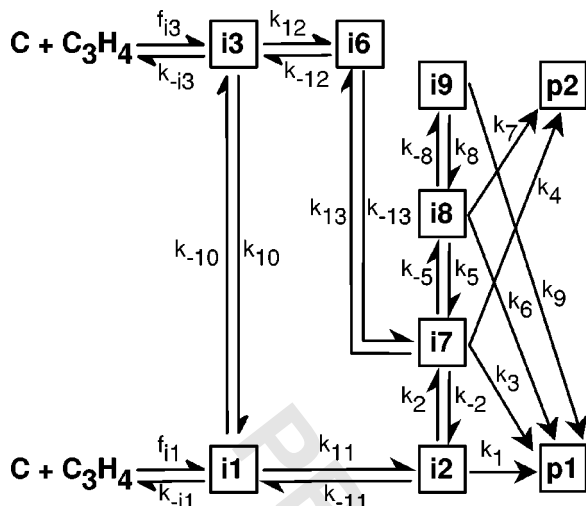


FIG. 4. Enhanced chemical kinetic scheme.

species except that in the latter case a shallower well depth of $D_e = 48.44 \text{ kcal/mol} = 16942 \text{ cm}^{-1}$ is employed. These well depths, correspond to the difference between *ab initio* energies with zero-point energies subtracted, calculated at the G2M level as depicted in Fig. 1.

In the μ VTST calculations, the location of the variationally determined transition states stayed well within the range $2.0 < R < 11.5 \text{ \AA}$. In addition, the μ VTST rate coefficient was found not to be sensitive to the value of R_{CMX} . These observations indicate that the current level of sophistication of the PES is more than adequate.

III. ENHANCED CHEMICAL KINETIC SCHEME

A. Solution

The original chemical kinetic scheme used in the previous work on the C(³P) + allene (C₃H₄) system is depicted in Fig. 15 of Ref. 2. In this treatment, the total input flux F was unknown and the possibility of species $i1$ and $i3$ dissociating via the entrance channel was disregarded. Thus, only relative branching ratios could be calculated and not total bimolecular reaction rates and partial capture rates.

In the current work, the chemical kinetic scheme has now been enhanced, as shown in Fig. 4, to allow for a theoretically predicted overall input flux F and also to allow for the possibility of redissociation via the entrance channels. The corresponding rate equations are

$$\frac{d[i1]}{dt} = -(k_{-10} + k_{11} - k_{-i1})[i1] + k_{-11}[i2] + k_{10}[i3] + f_{i1}, \quad (4)$$

$$\frac{d[i2]}{dt} = k_{11}[i1] - (k_1 + k_2 + k_{-11})[i2] + k_{-2}[i7], \quad (5)$$

$$\frac{d[i3]}{dt} = k_{-10}[i1] - (k_{10} + k_{12} - k_{-i3})[i3] + k_{-12}[i6] + f_{i3}, \quad (6)$$

$$\frac{d[i6]}{dt} = k_{12}[i3] - (k_{-12} + k_{-13})[i6] + k_{13}[i7], \quad (7)$$

$$\frac{d[i7]}{dt} = k_2[i2] + k_{-13}[i6] - (k_{-2} + k_{-5} + k_3 + k_4 + k_{13}) \times [i7] + k_5[i8], \quad (8)$$

$$\frac{d[i8]}{dt} = k_{-5}[i7] - (k_5 + k_6 + k_7 + k_{-8})[i8] + k_8[i9], \quad (9)$$

$$\frac{d[i9]}{dt} = k_{-8}[i8] - (k_8 + k_9)[i9], \quad (10)$$

whence the original chemical kinetic scheme of Ref. 2 is recovered for $k_{-i1} = k_{-i3} = 0$.

Since it is not easily possible to separate the overall input flux into contributions for each entrance channel species $i1$ and $i3$ we simply calculate the overall input flux F based on species $i1$ and perform calculations using a tuning parameter α .³⁸ On the basis of transition state theory,⁴ we can assume that the total input flux F at each E, J level is proportional to $W(E, J)$. The total input flux F can thus be expressed as the sum of the two individual fluxes

$$F = f_{i1} + f_{i3} \quad (11)$$

so that each entrance channel has an individual flux in terms of the tuning parameter α ,

$$f_{i1} \propto \alpha W(E, J), \quad (12)$$

$$f_{i3} \propto (1 - \alpha) W(E, J), \quad (13)$$

with a constant of proportionality related to the statistical weight of the E, J level. Merely for the purposes of obtaining a thermal bimolecular rate coefficient $k(T)$ (and not thereby making any assumptions about the experimental conditions studied in Ref. 2) we will assume a thermal input distribution so that the above fluxes will get a Boltzmann weighting. The calculation of the thermal bimolecular rate coefficient $k(T)$ is further discussed in Sec. IV B.

Since we are assuming collision free conditions, the species begin and remain on a fixed E, J level. Thus, the rate equations for the interconversion of species on each E, J level can be cast into matrix form as

$$\frac{d\mathbf{p}}{dt} = \mathbf{K}\mathbf{p} + \mathbf{f}, \quad (14)$$

where the population vector for the intermediates

$$\mathbf{p} = ([i1], [i2], [i3], [i6], [i7], [i8], [i9]), \quad (15)$$

the input flux vector (only nonzero for the starting intermediates $i1$ and $i3$),

$$\mathbf{f} = (f_{i1}, 0, f_{i3}, 0, 0, 0, 0), \quad (16)$$

but now the corresponding rate matrix \mathbf{K} is updated to account for the reverse dissociations (rate constants k_{i1} and k_{i3}) for the entrance channels

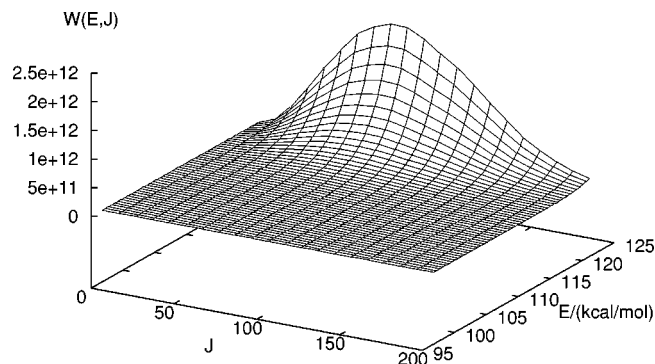


FIG. 5. Sum of states $W(E,J)$ for variational transition state for bimolecular entrance channel $C + C_3H_4$ (allene) $\rightarrow i1$.

ratios can be determined from the integrated product yields and the values obtained will be identical to those from the current approach.

B. Time evolution of the unimolecular system

If we treat the chemical kinetic system as a unimolecular reaction system, with initial population $(i1, i3)$ it is possible to obtain time resolved branching ratios from a time evolution of the system. Given long enough time, the system should evolve such that the same branching ratios (as population ratios) are obtained as predicted by a steady state solution for long times (Fig. 5). Additionally one can fit the time evolution of the production of product $p1$, approximately as a single exponential process, and obtain approximate effective rate constants k_{eff} and half-times $\tau_{1/2}$ for the production of $p1$. This information is tabulated in Table XI and some sample time evolutions using elementary rate constants $k(E, J)$ with $J=0$ are given in Fig. 6 for a collision energy of 19.6 kJ/mol (424.4 kJ/mol = 101.38 kcal/mol above the zero-point level of the $i2$ intermediate).

It is abundantly clear from an examination of Fig. 6, that the time evolution of reactants proceeds largely via the intermediate $i2$, regardless of the initial composition $(i1, i3)$. In fact, $i2$ is always important and $i7$ is clearly becoming less important, consistent with $p1$ being the major product and $p2$ being a much more minor product, as the initial population of $i1$ is increased.

The effect of reversibility, in allowing for redissociation of $i1$ and $i3$ species via the entrance channels into reactant species $C + \text{allene}$ (species $c+a$ in Figs. 6), is relatively minor but becomes more important as the collision energy is increased or as the initial flux into the $i3$ entrance channel is increased. This behavior is a consequence of the lower well depth for the $i3$ species relative to the $i1$ species. However, for the present system, the $i1$ entrance channel is likely to be the dominant one and so the effect of neglecting/treating reversibility in the entrance is negligible except at very high collision energies.

C. Branching ratios

In order to calculate the branching ratios it is necessary to carefully define what is meant by a branching ratio.³¹ The current kinetic scheme (resembling a chemical activation

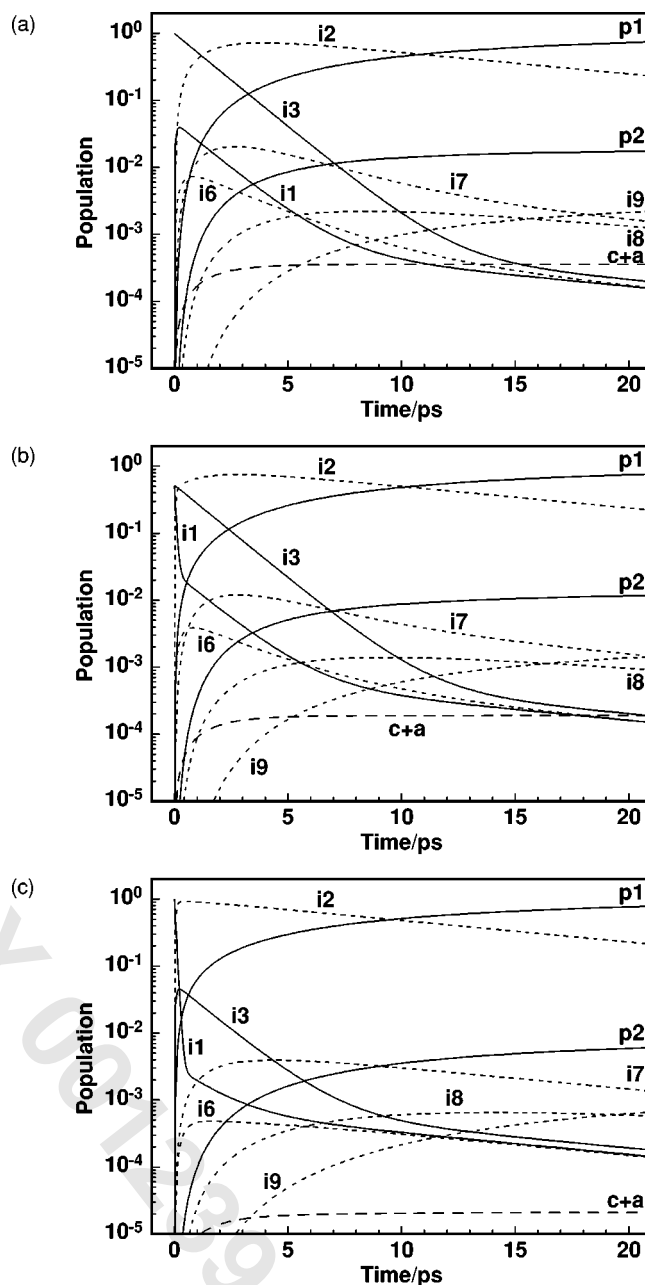


FIG. 6. Time evolution of unimolecular kinetic system calculated with microcanonical rate constants at $J=0$ and $E=101.38$ kcal/mol: (a) initial composition $(i1, i3) = (0, 1)$, (b) initial composition $(i1, i3) = (0.5, 0.5)$, (c) initial composition $(i1, i3) = (1, 0)$.

system) has an input flux (or fluxes) to form the two initial intermediates $i1$ and $i3$ and then these species can interconvert and convert to other intermediates on the way to finally and irreversibly form products. In the present system the parameter α can be tuned to measure the response of the chemical kinetic system in terms of product yields given a certain total input flux F .

The most obvious way to define a branching ratio is in terms of the overall flux $f(\rightarrow P)$ and partial fluxes $f(I \rightarrow P)$ to form products P which we can determine from the kinetic scheme. For the formation of product $p1$ the fluxes are

$$f(i2 \rightarrow p1) = k_1[i2], \quad (21)$$

$$f(i7 \rightarrow p1) = k_3[i7], \quad (22)$$

$$f(i8 \rightarrow p1) = k_6[i8], \quad (23)$$

$$f(i9 \rightarrow p1) = k_9[i9], \quad (24)$$

$$f(\rightarrow p1) = k_1[i2] + k_3[i7] + k_6[i8] + k_9[i9], \quad (25)$$

and for the formation of product $p2$ the fluxes are

$$f(i7 \rightarrow p2) = k_4[i7], \quad (26)$$

$$f(i8 \rightarrow p2) = k_7[i8], \quad (27)$$

$$f(\rightarrow p2) = k_4[i7] + k_7[i8]. \quad (28)$$

Thus, partial and overall branching ratios may be defined relative to the total input flux F ,

$$b(i2 \rightarrow p1) = f(i2 \rightarrow p1)/F, \quad (29)$$

$$b(i7 \rightarrow p1) = f(i7 \rightarrow p1)/F, \quad (30)$$

$$b(i8 \rightarrow p1) = f(i8 \rightarrow p1)/F, \quad (31)$$

$$b(i9 \rightarrow p1) = f(i9 \rightarrow p1)/F, \quad (32)$$

$$b(\rightarrow p1) = f(\rightarrow p1)/F, \quad (33)$$

$$b(i7 \rightarrow p2) = f(i7 \rightarrow p2)/F, \quad (34)$$

$$b(i8 \rightarrow p2) = f(i8 \rightarrow p2)/F, \quad (35)$$

$$b(\rightarrow p2) = f(\rightarrow p2)/F. \quad (36)$$

$$b(\rightarrow p2) = f(\rightarrow p2)/F. \quad (37)$$

In Ref. 2 another definition of branching ratio was employed, relative to the total product yield of $p2$. However, since the yield (flux) of $p2$ $f(\rightarrow p2)$ is very low, ratios involving it are, statistically speaking, highly unstable quantities to calculate and it would be more prudent to display the results as branching ratios referenced to the total input flux. It should be noted that, for the original chemical kinetic scheme of Ref. 2 which disallows redissociation ($k_{-i1} = k_{-i3} = 0$), at steady state the input flux must equal the output flux,

$$F = f_{i1} + f_{i3} = f(\rightarrow p1) + f(\rightarrow p2) \quad (38)$$

since there are no other sources and sinks. Thus, knowledge of F and the ratio $f(\rightarrow p1)/f(\rightarrow p2)$ allows the calculation of $f(\rightarrow p1)$ and $f(\rightarrow p2)$ and the total branching ratios $b(\rightarrow p1)$ and $b(\rightarrow p2)$ can be recovered from the results in Tables IV–VI of Ref. 2.

Using the steady state populations $\mathbf{p}(\infty)$ from Eq. (20) we may calculate branching ratios referenced to the total input flux for each product species. For example, by summing over the fluxes at each E, J which yield either product $p1$ or $p2$ we have the respective branching ratios

$$b_{p1}(E, J) = k_1 p_{i2}(\infty) + k_3 p_{i7}(\infty) + k_6 p_{i8}(\infty) + k_9 p_{i9}(\infty), \quad (39)$$

$$b_{p2}(E, J) = k_4 p_{i7}(\infty) + k_7 p_{i8}(\infty). \quad (40)$$

In terms of branching ratios relative to the total input flux, (as defined above) results are presented in Tables V–XI.

Essentially the same trends seen above are seen more clearly with the comparisons between the previous work (Ref. 2), the traditional RRKM and the UNIRATE ($J=0$) results in Tables VI, VII, and VIII–X. As the ratio $i1:i3$ is increased, the proportion of product $p1$ increases.

Unlike traditional RRKM codes UNIRATE code has the ability to generate energy and angular momentum resolved elementary rate constants $k(E, J)$ which we can thus convert to energy and angular momentum resolved branching ratios. These results are given in Table V, and Tables VIII–XI.

The branching ratios appear insensitive to variations in angular momentum. Part of this insensitivity is likely due to cancellations in the branching ratios. The general trend is such that the branching ratios are consistent with those calculated by the traditional RRKM approach. The primary product $p1$ accounts for at least 97% of the initial flux, regardless of initial composition ($i1, i3$).

The branching ratios for formation of products $p1$ (major product) and $p2$ (minor product) are shown in Figs. 7 and 8 for tuning parameter values of $\alpha=0, 0.5$, and 1.0 . Even if all of the total input flux is entering via the $i3$ entrance channel ($\alpha=0$) this only enhances the formation of product $p2$ by a few percent. This is due to the rapid interconversion to $i1$ and then a facile conversion to product $p1$ via the intermediate isomer $i2$. More interesting is the effect of reversibility in the entrance channel upon the $p1$ branching ratio; at higher energies $E > 110$ kcal/mol (collision energies above 59 kJ/mol) for $\alpha=0$ about 15% of the flux redissociates. As α is tuned towards unity, more of the input flux is entering by the $i1$ channel and the formation of product $p1$ is enhanced by a few percent at the expense of product $p2$ and at the expense of a much lower redissociation probability.

IV. MICROCANONICAL VARIATIONAL TRANSITION STATE THEORY

A. Energy and angular momentum resolved elementary rate constants

In order to proceed with the modeling of the enhanced kinetic scheme depicted in Fig. 4 and described in Sec. III it was necessary to estimate the elementary rate constants $k_1, k_2, \dots, k_8, k_9, k_{-i1}, k_{-i3}$ in the rate matrix \mathbf{K} . We do this via the TST theory,^{4–6}

$$k(E, J) = \frac{W(E, J)}{h\rho(E, J)}. \quad (41)$$

For 20 of the elementary steps which have explicit barriers (14 isomerizations and 6 eliminations) can be treated by tight μ -TST theory (flux minimizes at the barrier) to yield rate coefficients $k(E, J)$. However, in the current enhanced kinetic scheme the two loose entrance channels ($i1/i3$ recombination/fission) are explicitly treated. A proper treatment requires μ -VTST with the flux $W(E, J)/h$ variationally minimized as a function of the reaction coordinate. For the present calculation, we simply choose the reaction coordinate to be the center-of-mass separation of fragments. However, our theoretical approach, as implemented in our UNIRATE code,²⁵ allows for more generalized reaction co-

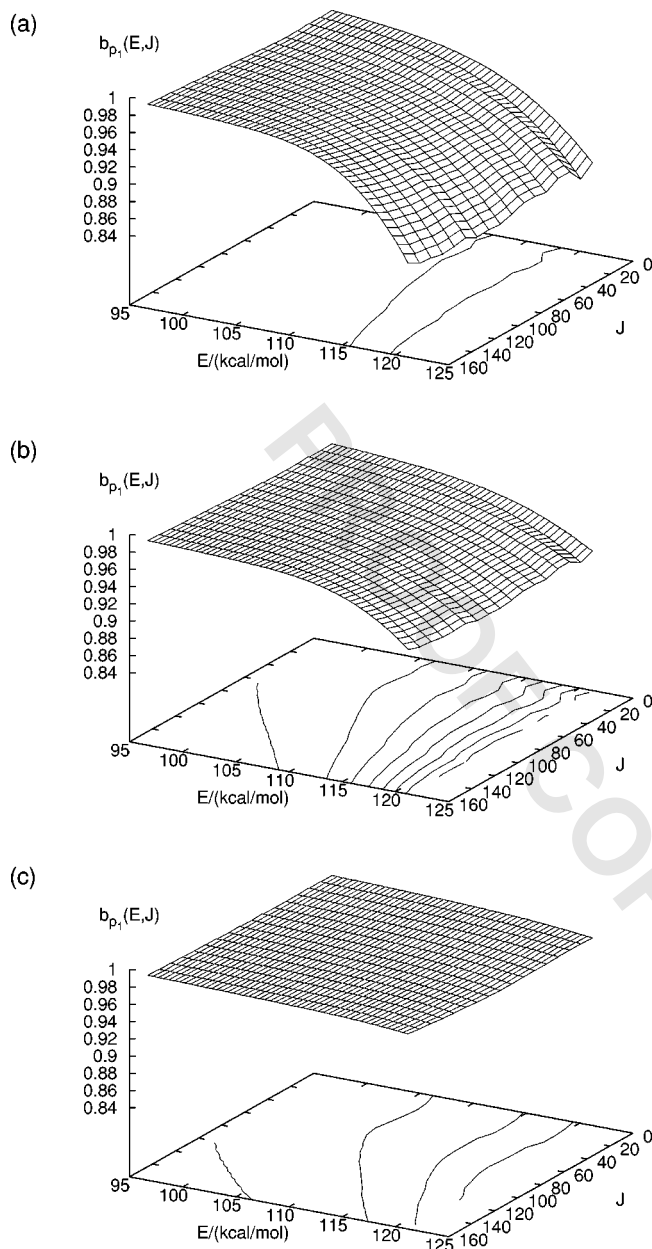


FIG. 7. Branching ratio $b_{p_1}(E, J)$ for formation of product p_1 : (a) initial composition $(i_1, i_3) = (0, 1)$, (b) initial composition $(i_1, i_3) = (0.5, 0.5)$, (c) initial composition $(i_1, i_3) = (1, 0)$.

ordinates. Details of the theoretical foundations of the UNIRATE package and further ongoing work can be found in Refs. 6.

To generate the required set of elementary rate constants using our UNIRATE package,²⁵ the corresponding set of molecular and transition state frequencies (in cm^{-1}) and rotational constants were based on those used in Ref. 3. The critical energies E_0 were obtained from the energies (in kcal/mol) displayed in Fig. 2 of Ref. 3 and Fig. 9 of Ref. 2. All energies of the intermediates were referenced to that of the lowest energy intermediate i_2 and the statistical calculations (UNIRATE) for each intermediate were matched so that they were run at the same total energy (collision energy) with respect to the lowest energy intermediate i_2 .

The energy and angular momentum resolved UNIRATE

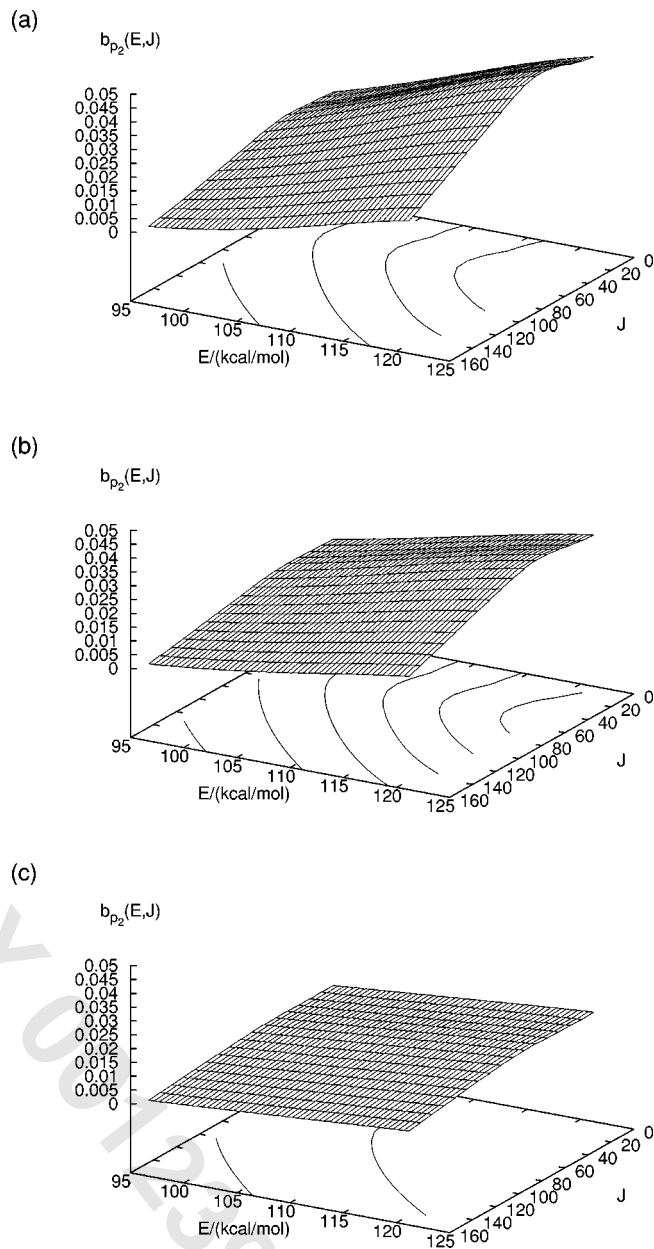


FIG. 8. Branching ratio $b_{p_2}(E, J)$ for formation of product p_2 : (a) initial composition $(i_1, i_3) = (0, 1)$, (b) initial composition $(i_1, i_3) = (0.5, 0.5)$, (c) initial composition $(i_1, i_3) = (1, 0)$.

calculation of the microcanonical rate coefficient $k(E, J)$ was run for a range of energies E focusing on energies in the neighborhood of the collision energies studied in the previous calculations,² and for a range of angular momentum, $J = 0-160$ which covers most of the range of the rotational peak in the overall angular momentum distribution.

The total input flux F in Eq. (11) was estimated using the i_1 channel predictions partitioned between each entrance channel as given in Eq. (12). The reverse dissociation unimolecular rate coefficients $k(E, J)$ for each entrance channel were similarly calculated to satisfy detailed balance. These calculations are facilitated by using the UNIRATE code²⁵ to predict sums of states $W(E, J)$ and unimolecular rate coefficients $k(E, J)$ for each elementary step.

For the loose entrance channels a number of models of

the transition state are available. The simplest level assumes free rotors in the loose transition state. A more sophisticated calculation, employs full Monte Carlo integration for the sum of states, with nonbonded interactions modeled by Lennard-Jones potentials, and the anisotropic potential modeled by the Coupled Sinusoidally Hindered Rotor (CSHR) model.⁷ Our most sophisticated calculations, however go beyond this approach by allowing for the calculation of the anisotropy for the entrance channel based on an explicit *ab initio* (DFT derived) model of the potential energy surface (discussed above in Sec. II B). The bulk of calculations presented here use this more sophisticated model, unless otherwise stated.

The potential importance of explicitly accounting for the energy and angular momentum dependence of unimolecular

TABLE I. Temperature dependence of the total thermal bimolecular reaction rate coefficient $k(T)/10^{-10} \text{ cm}^3 \text{ s}^{-1}$ for various models of the anisotropy in the entrance channel: Free, free rotor; CSHR, coupled sinusoidally hindered rotor; PES, based on the *ab initio* surface.

T/K	Free	CSHR	PES
50	1.75	1.50	1.33
75	2.59	2.23	2.03
100	3.21	2.79	2.57
150	3.98	3.51	3.28
200	4.45	3.94	3.72
300	5.05	4.42	4.26
400	5.47	4.66	4.61
500	5.79	4.78	4.88
600	6.07	4.84	5.10
700	6.30	4.86	5.28

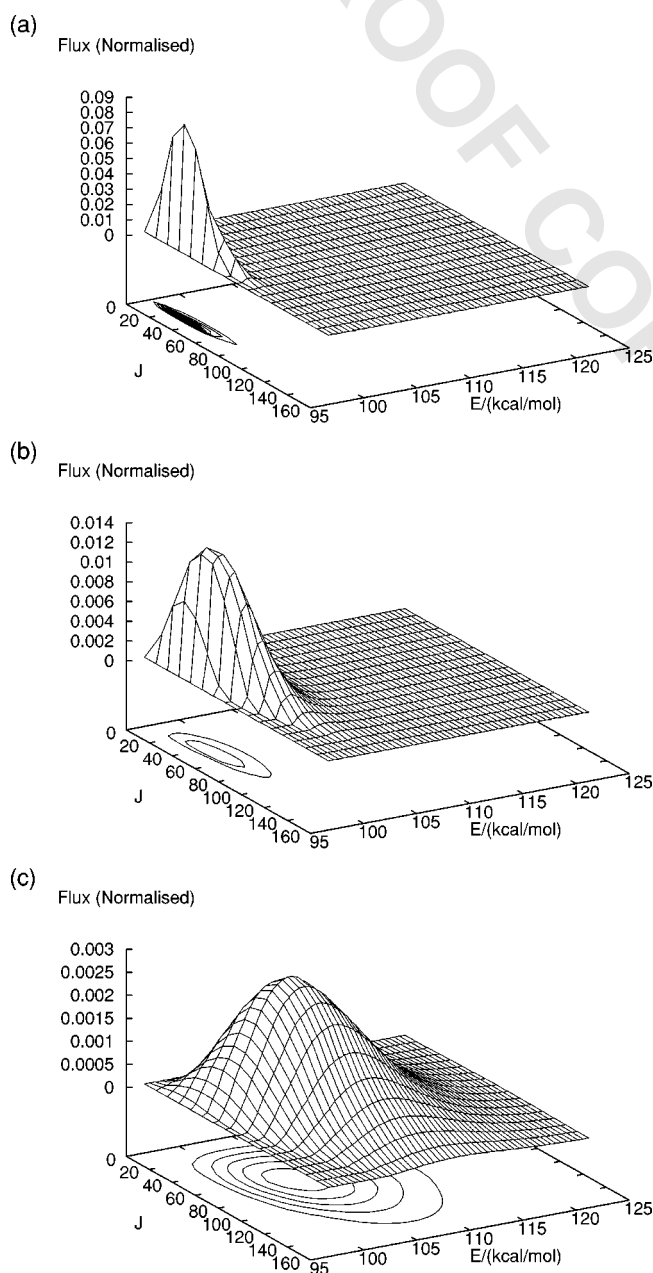


FIG. 9. Reaction flux distribution for formation of product $p1$ for $\alpha=0.0$: (a) at $T=100$ K, (b) at $T=300$ K, (c) at $T=700$ K.

rate coefficients is shown in Fig. 5 of the sum of states $W(E, J)$ for the bimolecular entrance channel $C + C_3H_4$ (allene) $\rightarrow i1$. There is significant J dependence present which would be ignored in a simple E -dependent RRKM calculation. This dependence could lead to significant effects on the total thermal bimolecular rate coefficient $k(T)$ though observed differences may be less due to the results of thermal averaging.

B. Thermal rate coefficients

Since the current theoretical approach now estimates the total input flux it is now possible to compute total reaction rates and partial capture rates. The total thermal bimolecular reaction rate coefficient can be readily computed as

$$k(T) = \frac{1}{hQ} \int_0^\infty dE \int_0^\infty dJ W(E, J) e^{-\beta E}, \quad (42)$$

where Q is the partition function for the incoming fragments. The thermal capture rate coefficient for product $p1$ is given in terms of the branching ratio $b_{p1}(E, J)$ by

$$k_{p1}(T) = \frac{1}{hQ} \int_0^\infty dE \int_0^\infty dJ W(E, J) e^{-\beta E} b_{p1}(E, J). \quad (43)$$

Thermal branching ratios can be computed from the ratios

$$b_{p1}(T) = \frac{k_{p1}(T)}{k(T)}. \quad (44)$$

Corresponding expressions for $k_{p2}(T)$ and $b_{p2}(T)$ apply for product $p2$.

Reaction flux distributions, essentially the normalized integrand in Eq. (43), are shown in Fig. 9 for temperatures of $T=100, 300,$ and 700 K. Clearly, at low temperatures, significant contributions to the thermal rate coefficient only arise for low energies $E \approx 97-100$ kcal/mol (where the threshold energy is 96.7 kcal/mol) and for $J \approx 10-80$.

The temperature dependence of the total thermal bimolecular coefficient $k(T)$ for the entrance channel of $C(^3P) + \text{allene}$ (C_3H_4) is shown in Table I and Fig. 10 for a number of models of the anisotropy. The simplest model (labeled Free) ignores the anisotropy and assumes free rotors in the loose transition state. An empirical model (labeled CSHR),

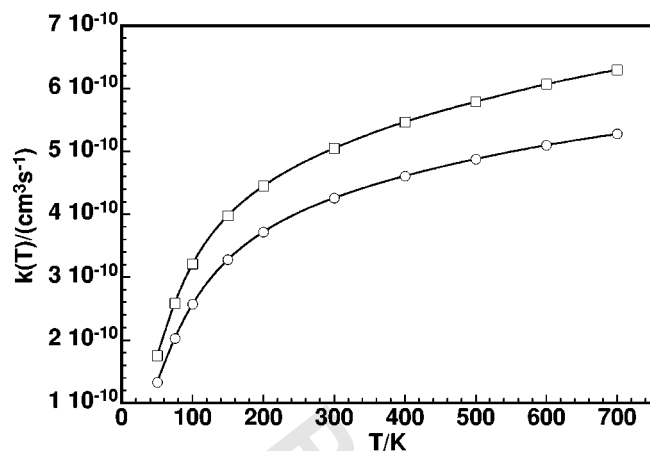


FIG. 10. Temperature dependence of the total thermal bimolecular reaction rate coefficient $k(T)$ for various models of the anisotropy in the entrance channel: Free, free rotor (□); PES, based on the *ab initio* surface (○).

employs an anisotropic potential modeled by the CSHR model⁷ with nonbonded interactions modeled by Lennard-Jones potentials. The most sophisticated calculation (labeled PES), employs full Monte Carlo integration for the sum of states, with non-bonded interactions modeled by Lennard-Jones potentials, with the anisotropic potential modeled by the *ab initio* (DFT derived) PES described in Sec. II B. The PES model yields substantially smaller thermal rate coefficients than for the free rotor predictions in in Table I and Fig. 10. Moving to lower temperatures, the thermal rate coefficients predicted by each of these models approach each other. This is a consequence of the E, J -dependent transition state location moving out to larger values of R (the center-of-mass separation of the fragments) in which region the potential energy surface approaches being equally flat for all of the models. Moving to higher temperatures, the E, J -dependent transition state locations move inwards to lower values of R . In this region the different models have different models of the anisotropy arising from the potential

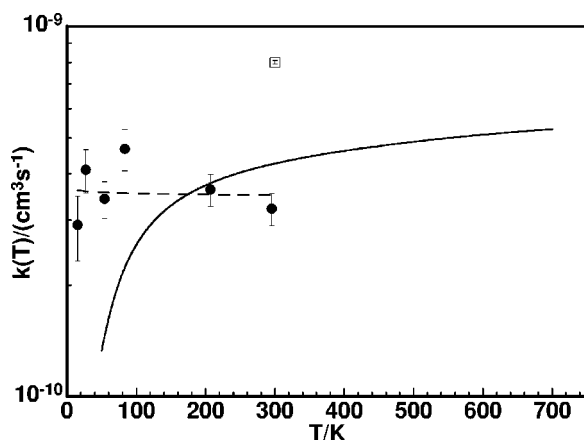


FIG. 11. Temperature dependence of the total thermal bimolecular reaction rate coefficient $k(T)$ from experimental results of Chastaing *et al.* (Refs. 33, 34) (●) and Husain *et al.* (Ref. 35) (□) compared with theoretical predictions (solid curve) based on the *ab initio* PES in the present work. The dashed line represents a fit to the equation $k(T) = AT^B$ for the results of Chastaing *et al.* (Refs. 33, 34).

TABLE II. Temperature dependence of the total thermal bimolecular reaction rate coefficient $k(T)/10^{-10} \text{ cm}^3 \text{ s}^{-1}$ based on experimental results of Chastaing *et al.* (Refs. 33, 34) ($T=15\text{--}295 \text{ K}$) and Husain *et al.* (Ref. 35) ($T=300 \text{ K}$) compared with theoretical predictions based on the *ab initio* PES in the present work.

T/K	Experiment	Theory
15	2.91 ± 0.58	
27	4.10 ± 0.55	
54	3.42 ± 0.39	1.46
83	4.67 ± 0.60	2.23
207	3.63 ± 0.36	3.76
295	3.22 ± 0.32	4.25
300	8.0 ± 0.01	4.27

of interaction between the approaching C+ allene fragments. The Free model has no hindering; the CSHR and PES models assume a hindering potential respectively based either on a particular functional form⁷ or on *ab initio* data and thus lead to lower estimates of the thermal rate coefficients as the temperature is raised. At the highest temperatures examined, the empirical CSHR model apparently assumes too much hindering and leads to a cross over below the PES model to predict a lower thermal capture rate coefficient.³²

Comparison of the theoretical thermal rate coefficient $k(T)$ predictions of the PES model with recent experimental results of Chastaing *et al.*^{33,34} and Husain *et al.*³⁵ is made in Fig. 11 and Table II. Agreement is within a factor of 2 above $T=60 \text{ K}$. The theoretical predictions apparently show a more pronounced temperature dependence than the experimental results of Chastaing *et al.*,^{33,34} with the former fitted by a form $k(T) = (2.68 \pm 0.12) \times 10^{-10} (T/\text{K})^{-(0.116 \pm 0.007)} \times e^{-(57.54 \pm 1.33 \text{ K})/T} \text{ cm}^3 \text{ s}^{-1}$ and the latter fitted to the form $(3.5 \pm 0.8) \times 10^{-10} (T/\text{K})^{-(0.01 \pm 0.12)} \text{ cm}^3 \text{ s}^{-1}$. The increasing discrepancy in the very low temperature regime may be due to inaccuracies in our PES model for large transition state separations. Low temperature rates are dominated by the long range PES. In this regime a better approach may be to use a low-temperature capture model such as those developed by Bettens *et al.*^{36,37} for similar systems.

TABLE III. Thermal branching ratio $b_p(T)$ as a function of the temperature T/K and the tuning parameter α . Results are given for the formation of product $n\text{-C}_4\text{H}_3$ (p_1) and $i\text{-C}_4\text{H}_3$ (p_2).

T/K	α	$b_{p_1}(T)$	$b_{p_2}(T)$
100	0.0	0.984	0.0159
	0.5	0.987	0.0113
	1.0	0.993	0.0067
300	0.0	0.984	0.0172
	0.5	0.988	0.0121
	1.0	0.993	0.0071
500	0.0	0.979	0.0199
	0.5	0.988	0.0139
	1.0	0.992	0.0079
700	0.0	0.977	0.0241
	0.5	0.983	0.0165
	1.0	0.992	0.0089

TABLE IV. A comparison of the previous work (Ref. 2), UNIRATE and RRKM12 predictions of the microcanonical rate coefficient $k(E, J=0)$ at a collision energy of 19.6 kJ/mol (424.4 kJ/mol=101.38 kcal/mol above the zero-point level of the $i2$ intermediate) for the elementary reaction of $i2$ to form $i1$ in the C+C₃H₄ (allene) system. The IAMS rate constants are from Ref. 2 except that a correction has been made such that k_5, k_8, k_{13} have been swapped with k_{-5}, k_{-8}, k_{-13} .

Rate constant/s ⁻¹	Ref. 2	RRKM12	UNIRATE ($J=0$)
k_1	2.91×10^{11}	7.423×10^{10}	7.281×10^{10}
k_2	8.26×10^9	1.977×10^9	1.913×10^9
k_{-2}	7.41×10^{10}	7.327×10^{10}	7.049×10^{10}
k_3	1.75×10^{11}	1.807×10^{11}	1.760×10^{11}
k_4	2.24×10^{11}	1.108×10^{11}	1.093×10^{11}
k_5	3.28×10^9	3.430×10^9	3.295×10^9
k_{-5}	2.88×10^{10}	2.880×10^{10}	2.868×10^{10}
k_6	2.88×10^{10}	2.894×10^{10}	2.838×10^{10}
k_7	3.20×10^9	1.610×10^9	1.631×10^9
k_8	7.61×10^9	2.890×10^9	2.722×10^9
k_{-8}	6.03×10^{10}	5.542×10^{10}	6.723×10^{10}
k_9	1.14×10^9	4.377×10^8	3.581×10^8
k_{10}	1.13×10^{12}	5.633×10^{11}	6.473×10^{11}
k_{-10}	7.18×10^{11}	7.219×10^{11}	7.426×10^{11}
k_{11}	1.34×10^{13}	1.327×10^{13}	1.349×10^{13}
k_{-11}	1.86×10^{10}	9.647×10^9	9.002×10^9
k_{12}	5.04×10^{10}	2.561×10^{10}	2.844×10^{10}
k_{-12}	1.57×10^{10}	7.888×10^9	8.203×10^9
k_{13}	2.50×10^{11}	2.434×10^{11}	2.582×10^{11}
k_{-13}	4.92×10^{12}	2.468×10^{12}	2.628×10^{12}
k_{-i1}			8.756×10^6
k_{-i3}			2.295×10^8

Thermal branching ratios $b_{p1}(T)$ and $b_{p2}(T)$ are given in Table III as a function of temperature T and tuning parameter α . Clearly, the major product $p1$ dominates with more than $\approx 98\%$ of the product yield. Only as α is lowered and the temperature T is raised does the yield of $p2$ become more than 2%.^{38,39}

V. COMPARISON WITH PREVIOUS WORK

In this section we describe calculations performed for comparison with the results of previous work.² In this previous work, the RRKM rate constants were tabulated in Table 3 of Ref. 2 for two collision energies (Table IV).⁴⁰ In the comparisons, we focus on calculations at the lower collision energy of 19.6 kJ/mol (424.4 kJ/mol=101.38 kcal/mol above

TABLE V. Comparison table (Ref. 2, RRKM, UNIRATE with $J=0$) for branching to i -C₄H₃ ($p2$) at $E=101.38$ kcal/mol (collision energy of 19.6 kJ/mol).

($i1, i3$)	Ref. 2	RRKM12	$J=0$
(0.00, 1.00)	0.032	0.020	0.020
(0.10, 0.90)	0.030	0.019	0.019
(0.20, 0.80)	0.029	0.018	0.017
(0.30, 0.70)	0.027	0.017	0.016
(0.40, 0.60)	0.025	0.015	0.015
(0.50, 0.50)	0.023	0.014	0.014
(0.60, 0.40)	0.021	0.013	0.013
(0.70, 0.30)	0.019	0.012	0.012
(0.80, 0.20)	0.017	0.011	0.010
(0.90, 0.10)	0.015	0.009	0.009
(1.00, 0.00)	0.014	0.008	0.008

TABLE VI. Corrected results of Ref. 2 using normal branching ratio definition for branching $\rightarrow p1$ at $E=101.38$ kcal/mol (collision energy of 19.6 kJ/mol).

($i1, i3$)	$i2 \rightarrow p1$	$i7 \rightarrow p1$	$i8 \rightarrow p1$	$i9 \rightarrow p1$	$\rightarrow p1$
(0.00, 1.00)	0.939	0.025	0.003	0.001	0.968
(0.10, 0.90)	0.943	0.024	0.003	0.001	0.970
(0.20, 0.80)	0.946	0.022	0.002	0.001	0.971
(0.30, 0.70)	0.950	0.021	0.002	0.001	0.973
(0.40, 0.60)	0.953	0.019	0.002	0.001	0.975
(0.50, 0.50)	0.957	0.018	0.002	0.001	0.977
(0.60, 0.40)	0.960	0.016	0.002	0.000	0.979
(0.70, 0.30)	0.964	0.015	0.002	0.000	0.981
(0.80, 0.20)	0.967	0.013	0.001	0.000	0.983
(0.90, 0.10)	0.971	0.012	0.001	0.000	0.985
(1.00, 0.00)	0.974	0.011	0.001	0.000	0.986

the zero-point level of the $i2$ intermediate) since the results at the higher collision energy 38.8 kJ/mol (443.4 kJ/mol =105.98 kcal/mol above the zero-point level of the $i2$ intermediate) are substantially similar. Correctly recalculated results of the previous work are presented in Tables V and VI using the branching ratios as defined in Sec. III C.⁴¹

From these results, it is clear that $p1$ is the primary product even as the composition ($i1, i3$) is varied, with most of the flux traversing the pathway involving $i2$. The trends are such that $p1:p2$ branching ratios increase with increasing $i1:i3$ ratios. This is the opposite of the trend depicted in Ref. 2. The results in Table IV–VI of Ref. 2 show $p1/p2$ ratios that are decreasing as the $i1/i3$ ratio is increasing; one would have expected the reverse. The only way that that $i3$ could be preferred to $i1$ for producing $p1$ is if the rate constants were larger via $i3$ to get to $p1$ than from $i1$ to $p1$. Taking the most direct (independent) route, at a collision energy of 19.6 kJ/mol (101.38 kcal/mol above $i2$ zero point) using the rate constants, the path $i3 \rightarrow i6 \rightarrow i7 \rightarrow p1$ involves the rate constants $k_{12}, k_{-12}, k_{13}, k_{-13}$, and k_3 whereas the path $i1 \rightarrow i2 \rightarrow p1$ involves the rate constants $k_{10}, k_{-10}, k_{11}, k_{-11}$, and k_1 . Examining the magnitude of rate constants in Table IV it is clear that the pathway from $i1 \rightarrow p1$ seems the most direct (two steps) and quickest ($i2$ is the major intermediate and $i7$ is about 1–2 orders of magnitude lower in concentration).

TABLE VII. RRKM branching ratios for branching $\rightarrow p1$ at $E=101.38$ kcal/mol (collision energy of 19.6 kJ/mol).

($i1, i3$)	$i2 \rightarrow p1$	$i7 \rightarrow p1$	$i8 \rightarrow p1$	$i9 \rightarrow p1$	$\rightarrow p1$
(0.00, 1.00)	0.942	0.033	0.004	0.001	0.980
(0.10, 0.90)	0.946	0.031	0.003	0.001	0.981
(0.20, 0.80)	0.949	0.029	0.003	0.001	0.982
(0.30, 0.70)	0.953	0.027	0.003	0.001	0.983
(0.40, 0.60)	0.956	0.025	0.003	0.001	0.985
(0.50, 0.50)	0.960	0.023	0.003	0.001	0.986
(0.60, 0.40)	0.963	0.021	0.002	0.001	0.987
(0.70, 0.30)	0.966	0.019	0.002	0.001	0.988
(0.80, 0.20)	0.970	0.017	0.002	0.000	0.989
(0.90, 0.10)	0.973	0.015	0.002	0.000	0.991
(1.00, 0.00)	0.977	0.013	0.001	0.000	0.992

TABLE VIII. UNIRATE branching ratios for branching $\rightarrow p1$ at $E = 101.38$ kcal/mol (collision energy of 19.6 kJ/mol) and $J=0$.

$(i1,i3)$	$i2 \rightarrow p1$	$i7 \rightarrow p1$	$i8 \rightarrow p1$	$i9 \rightarrow p1$	$\rightarrow p1$
(0.00, 1.00)	0.943	0.032	0.004	0.001	0.980
(0.10, 0.90)	0.947	0.030	0.003	0.001	0.981
(0.20, 0.80)	0.950	0.028	0.003	0.001	0.982
(0.30, 0.70)	0.953	0.026	0.003	0.001	0.983
(0.40, 0.60)	0.957	0.024	0.003	0.001	0.985
(0.50, 0.50)	0.960	0.022	0.003	0.001	0.986
(0.60, 0.40)	0.964	0.021	0.002	0.001	0.987
(0.70, 0.30)	0.967	0.019	0.002	0.001	0.988
(0.80, 0.20)	0.970	0.017	0.002	0.001	0.989
(0.90, 0.10)	0.974	0.015	0.002	0.000	0.991
(1.00, 0.00)	0.977	0.013	0.001	0.000	0.992

VI. CONCLUSIONS

We have successfully demonstrated a methodology which allows for full energy and angular momentum resolution of rate coefficients and branching ratios. In addition, the ability to handle the initial capture processes means that the computation of total thermal bimolecular reaction rates and partial capture rates is now possible. The theoretical approach used, as implemented in program UNIRATE,²⁵ also allows for the development of more generalized reaction coordinates to handle multiple entrance and exit channel systems (Tables VII–XI).

In this work we have been using the $C(^3P)+$ allene (C_3H_4) reaction as a test system. The previous work² and the current calculations are in substantial agreement for the calculation of the microcanonical rate constants for the elementary reactions in the $C+C_3H_4$ (allene) kinetic scheme. This agreement relies on the rate constants in Table 3 of Ref. 2 being corrected such that k_5, k_8, k_{13} is swapped with k_{-5}, k_{-8}, k_{-13} . The general conclusion, that $p1$ is the major product, independent of composition $(i1,i3)$ is still valid, even when accounting for angular momentum conservation. The effect of angular momentum conservation on branching ratios appears to be minor at the energies studied.

The effect of reversibility in the entrance channel on the product branching is small in this system, except when going to higher collision energies. This is also true in the of the corresponding thermally averaged capture rate constants and thermal branching ratios. Other chemical systems may show

TABLE IX. UNIRATE branching ratios for branching $\rightarrow p1$ at $E = 105.98$ kcal/mol (collision energy of 38.8 kJ/mol) and $J=0$.

$(i1,i3)$	$i2 \rightarrow p1$	$i7 \rightarrow p1$	$i8 \rightarrow p1$	$i9 \rightarrow p1$	$\rightarrow p1$
(0.00, 1.00)	0.933	0.036	0.004	0.001	0.974
(0.10, 0.90)	0.937	0.034	0.004	0.001	0.976
(0.20, 0.80)	0.941	0.031	0.004	0.001	0.977
(0.30, 0.70)	0.945	0.029	0.003	0.001	0.979
(0.40, 0.60)	0.950	0.027	0.003	0.001	0.981
(0.50, 0.50)	0.954	0.025	0.003	0.001	0.982
(0.60, 0.40)	0.958	0.022	0.003	0.001	0.984
(0.70, 0.30)	0.962	0.020	0.002	0.001	0.985
(0.80, 0.20)	0.966	0.018	0.002	0.001	0.987
(0.90, 0.10)	0.971	0.016	0.002	0.000	0.989
(1.00, 0.00)	0.975	0.013	0.002	0.000	0.990

TABLE X. UNIRATE branching ratios for branching $\rightarrow p1$ at $E = 110.70$ kcal/mol (collision energy of 58.6 kJ/mol) and $J=0$.

$(i1,i3)$	$i2 \rightarrow p1$	$i7 \rightarrow p1$	$i8 \rightarrow p1$	$i9 \rightarrow p1$	$\rightarrow p1$
(0.00, 1.00)	0.910	0.040	0.005	0.001	0.956
(0.10, 0.90)	0.916	0.037	0.005	0.001	0.959
(0.20, 0.80)	0.922	0.034	0.004	0.001	0.962
(0.30, 0.70)	0.928	0.032	0.004	0.001	0.965
(0.40, 0.60)	0.935	0.029	0.004	0.001	0.968
(0.50, 0.50)	0.941	0.027	0.003	0.001	0.972
(0.60, 0.40)	0.947	0.024	0.003	0.001	0.975
(0.70, 0.30)	0.953	0.022	0.003	0.001	0.978
(0.80, 0.20)	0.959	0.019	0.002	0.001	0.981
(0.90, 0.10)	0.966	0.016	0.002	0.001	0.985
(1.00, 0.00)	0.972	0.014	0.002	0.000	0.988

a greater effect, especially if they involve entrance channels with shallow wells under conditions of high collision energies.

We have also successfully implemented the *ab initio* entrance channels, shown in Figs. 2(b) and 2(b) into the theoretical calculation. A major goal is now to use the techniques developed in this project to model other complex reactions of interest.

ACKNOWLEDGMENTS

This work was facilitated by the collaborative program between the Computational Molecular Science Group at the University of Queensland and the Institute of Atomic and Molecular Sciences, Academia Sinica, Taiwan. Professor S. H. Lin is thanked for his hospitality and stimulating discussions during visits to the IAMS by one of the authors (H.W.S.) in September 1999 and February 2001. Portions of this work benefited from substantial computational resources provided by the Supercomputer Facility at the Australian National University. We also thank the Australian Research Council for ongoing support.

TABLE XI. Total branching $\rightarrow p1$ calculated from our Fortran code compared with results of the stochastic CKS package (Ref. 29) and the deterministic REACT package (Ref. 30). Fitted first order rate constants and half-lives are given for the formation of the major product $p1$.

Calculation	$(i1,i3)$	CKS,			
		Fortran	REACT	$k_{\text{eff}}/\text{ps}^{-1}$	$\tau_{1/2}/\text{ps}$
Ref. 2	(0.00, 1.00)	0.968	0.968	0.185	5.41
	(0.50, 0.50)	0.977	0.977	0.227	4.41
	(1.00, 0.00)	0.986	0.987	0.278	3.60
RRKM	(0.00, 1.00)	0.980	0.980	0.0583	17.1
	(0.50, 0.50)	0.986	0.986	0.0658	15.2
	(1.00, 0.00)	0.992	0.992	0.0739	13.5
UNIRATE ($J=0$)	(0.00, 1.00)	0.980	0.978	0.0592	16.9
	(0.50, 0.50)	0.986	0.986	0.0657	15.2
	(1.00, 0.00)	0.992	0.992	0.0726	13.8
UNIRATE ($J=50$)	(0.00, 1.00)	0.977	0.977	0.0605	16.5
	(0.50, 0.50)	0.984	0.985	0.0674	14.8
	(1.00, 0.00)	0.991	0.992	0.0747	13.4

- ¹R. I. Kaiser, D. Stranges, Y. T. Lee, and A. G. Suits, *J. Chem. Phys.* **105**, 8721 (1996).
- ²R. I. Kaiser, A. M. Mebel, A. H. H. Chang, S. H. Lin, and Y. T. Lee, *J. Chem. Phys.* **110**, 10 330 (1999).
- ³A. M. Mebel, R. I. Kaiser, and Y. T. Lee, *J. Am. Chem. Soc.* **122**, 1776 (2000).
- ⁴W. H. Miller, *J. Chem. Phys.* **61**, 1823 (1974); D. G. Truhlar and B. C. Garrett, *Acc. Chem. Res.* **13**, 440 (1980); P. Pechukas, *Annu. Rev. Phys. Chem.* **32**, 159 (1981).
- ⁵H. W. Schranz, L. M. Raff, and D. L. Thompson, *Chem. Phys. Lett.* **171**, 68 (1990).
- ⁶S. C. Smith, *J. Phys. Chem.* **97**, 7034 (1993); *J. Chem. Phys.* **98**, 6496 (1994); **106**, 9236 (1997); **111**, 1830 (1999); *J. Phys. Chem. A (C. B. Moore, special edition)* **104**, 10 489 (2000).
- ⁷S. C. Smith, *J. Phys. Chem.* **95**, 3404 (1991).
- ⁸E. W.-G. Diau and S. C. Smith, *J. Chem. Phys.* **106**, 9236 (1997); E. W.-G. Diau and S. C. Smith, *J. Phys. Chem.* **100**, 12 349 (1996).
- ⁹T. J. Frankcombe and S. C. Smith, *Faraday Discuss.* **119**, 159 (2002).
- ¹⁰J. R. Barker, *Int. J. Chem. Kinet.* **33**, 232 (2001); John R. Barker and Nicolas F. Ortiz, *ibid.* **33**, 246 (2001); J. R. Barker, L. M. Yoder, and K. D. King, *J. Phys. Chem. A* **105**, 796 (2001).
- ¹¹S. J. Klippenstein, A. F. Wagner, S. H. Robertson, R. C. Dunbar, and D. M. Wardlaw, VARIFLEX, <http://chemistry.anl.gov/variflex>, 1999.
- ¹²D. K. Hahn, S. J. Klippenstein, and J. A. Miller, *Faraday Discuss.* **119**, 79 (2002).
- ¹³D.-C. Fang, L. B. Harding, S. J. Klippenstein, and J. A. Miller, *Faraday Discuss.* **119**, 207 (2002).
- ¹⁴L. Vereecken, G. Huyberechts, and J. Peeters, *J. Chem. Phys.* **106**, 6564 (1997).
- ¹⁵R. G. Susnow, A. M. Dean, W. H. Green, P. Peczak, and L. J. Broadbelt, *J. Phys. Chem. A* **101**, 3731 (1997); P. K. Venkatesh, A. M. Dean, M. H. Cohen, and R. W. Carr, *J. Chem. Phys.* **107**, 8904 (1997); P. K. Venkatesh, A. M. Dean, M. H. Cohen, and R. W. Carr, *ibid.* **111**, 8313 (1999).
- ¹⁶J. J. Lin, Y. T. Lee, and X. Yang, *J. Chem. Phys.* **113**, 1831 (1999).
- ¹⁷J. J. Jin, J. Shu, Y. T. Lee, and X. Yang, *J. Chem. Phys.* **113**, 5287 (1999).
- ¹⁸J. Shu, J. J. Jin, Y. T. Lee, and X. Yang, *J. Chem. Phys.* **113**, 9678 (1999).
- ¹⁹R. D. Kern, K. Xie, and H. Chen, *Combust. Sci. Technol.* **85**, 77 (1992); R. D. Smith, *Combust. Flame* **35**, 179 (1979); I. R. Slagle and D. Gutman, in *Proceedings of the 23rd Symposium on International Combustion Chemistry*, 1988, p. 875; L. R. Thorne, M. C. Branch, D. W. Chandler, R. J. Kee, and J. Miller, in *Proceedings of the 21st Symposium International Combustion Chemistry*, 1986, p. 965.
- ²⁰R. I. Kaiser, T. N. Le, Thanh L. Nguyen, A. M. Mebel, N. Balucani, Y. T. Lee, F. Stahl, P. v. R. Schleyer, and H. F. Schaefer III, *Faraday Discuss.* **119**, 51 (2002).
- ²¹Symposium on Titan, ESA-SP 338, ESTEC, Noordwijk, 1992.
- ²²E. Herbst, H. H. Lee, D. A. Howe, and T. J. Millar, *Mon. Not. R. Astron. Soc.* **268**, 335 (1994).
- ²³A. D. Becke, *J. Chem. Phys.* **98**, 5648 (1993).
- ²⁴A. M. Mebel, K. Morokuma, and M. C. Lin, *J. Chem. Phys.* **103**, 7414 (1995).
- ²⁵S. C. Smith, E. W.-G. Diau, and H. W. Schranz, UNIRATE, Energy and Angular Momentum Resolved Generalized Transition State Theory Fortran Code, 2001.
- ²⁶M. J. Frisch, G. W. Trucks, H. B. Schlegel *et al.*, GAUSSIAN 98, Revision A.9 (Gaussian, Inc., Pittsburgh, Pennsylvania, 1998).
- ²⁷S. Jeffrey, K. E. Gates, and S. C. Smith, *J. Phys. Chem.* **100**, 7090 (1996).
- ²⁸MATHEMATICA, Version 2.2 (Wolfram Research, Inc., Champaign, Illinois, 1993).
- ²⁹CKS, B. Hinsberg and F. A. Houle, IBM Research Division, Almaden Research Center, San Jose, California 95120-6099.
- ³⁰REACT, M. Whitbeck, *Tetrahedron Computer Methodology* **3**, 497 (1992).
- ³¹“When I use a word,” Humpty Dumpty said in rather a scornful tone, “it means just what I choose it to mean—neither more nor less.” Lewis Carroll, *Through the Looking-Glass and What Alice Found There*.
- ³²Harold W. Schranz, RRKM12, Strong Collision Assumption RRKM Fortran Code, 2001.
- ³³D. Chastaing, S. D. Le Picard, I. R. Sims, and I. W. M. Smith, *Astron. Astrophys.* **365**, 241 (2001).
- ³⁴D. Chastaing, S. D. Le Picard, I. R. Sims, I. W. M. Smith, W. D. Geppert, C. Naulin, and M. Costes, *Chem. Phys. Lett.* **331**, 170 (2000).
- ³⁵D. Husain and A. X. Ioannou, *J. Chem. Soc., Faraday Trans.* **93**, 3625 (1997).
- ³⁶R. P. A. Bettens and M. A. Collins, *J. Chem. Phys.* **116**, 101 (2002).
- ³⁷R. P. A. Bettens and M. A. Collins, *J. Chem. Phys.* **114**, 10342 (2001).
- ³⁸Comment: The overall input flux based on species *i3* is comparable to that based on species *i1*.
- ³⁹Since all populations of intermediates irreversibly decay to products *p1* and *p2*, so that the determinant of **K** is nonzero.
- ⁴⁰In the course of this work it was deduced that the rate constants in Table III of Ref. 2 should be corrected such that k_5 , k_8 , k_{13} is swapped with k_{-5} , k_{-8} , k_{-13} . It is likely that this error was caused by the numbering scheme used in Fig. 15 of Ref. 2, which usually (but not always) had lower numbered intermediates going *forward* to higher numbered intermediates.
- ⁴¹It should be noted, that the *p1:p2* branching ratios results in Table IV–VI of Ref. 2 are only correct for the last row, for composition (*i1,i3*) = (1,0), and that there is a substantial error in the remaining results. Upon recalculation it has been determined that (if it is not just a transcription error of the results to the tables) that the most likely source in the previous work (Ref. 2) is in the Laplace transform derived solutions (which involve complicated expressions) employed to generate the product populations at $t \rightarrow \infty$. Given the partial correctness of the results, it would appear that any terms involving the initial population of *i3* are incorrect or incomplete whereas the terms involving the initial population of *i1* are substantially correct. The former terms are substantially more complex than the latter terms (to a first approximation that k_2/k_{-2} are small). Given the complexity of solving a 7×7 rate matrix by hand, it is possible that there might be some error in the solutions. The current calculations have been checked in terms of the rate matrix used and independent methods of solution employed [Fortran, MATHEMATICA, and the Chemical Kinetic Simulator (Ref. 29)].